

Applying laser Doppler anemometry inside a Taylor–Couette geometry using a ray-tracer to correct for curvature effects

Sander G. Huisman*, Dennis P.M. van Gils, Chao Sun*

Physics of Fluids, Faculty of Science and Technology, Burgers Center for fluid dynamics, University of Twente, The Netherlands

ARTICLE INFO

Article history:

Received 21 July 2011
Received in revised form
1 February 2012
Accepted 27 March 2012
Available online 10 April 2012

Keywords:

Laser Doppler anemometry
Taylor–Couette
Curvature
Ray-tracer
Refraction
Correction

ABSTRACT

In the present work it will be shown how the curvature of the outer cylinder affects laser Doppler anemometry measurements inside a Taylor–Couette apparatus. The measurement position and the measured velocity are altered by curved surfaces. Conventional methods for curvature correction are not applicable to our setup, and it will be shown how a ray-tracer can be used to solve this complication.

By using a ray-tracer the focal position can be calculated, and the velocity can be corrected. The results of the ray-tracer are verified by measuring an a priori known velocity field, and after applying refractive corrections good agreement with theoretical predictions are found. The methods described in this paper are applied to measure the azimuthal velocity profiles in high Reynolds number Taylor–Couette flow for the case of outer cylinder rotation.

© 2012 Elsevier Masson SAS. All rights reserved.

1. Introduction

A Taylor–Couette (TC) apparatus consists of two coaxial, differentially rotating, cylinders, see Fig. 1. The annulus between the cylinders is filled with a working fluid; most commonly, as in our case, water is chosen. The apparatus has been used to study hydrodynamic instabilities, pattern formation, turbulence, and was found to have a rich phase diagram with different types of flow structures [1–11]. To get a deep understanding of these phenomena it is crucial to measure the local flow velocity.

Measuring the velocity field inside a TC apparatus was done for a long time using intrusive measurement techniques, e.g. constant temperature anemometry [12–15] and Pitot tubes [16]. Though these techniques are robust and proven to work, they are not ideal for measuring the velocity in TC flow. The aforementioned methods measure the magnitude of the velocity, not the individual components, and are directionally ambiguous using a single probe. Of course, one could use multiple probes [17] to obtain the flow direction. Another problem is that they alter the flow under consideration. Though this is not an issue for non-recirculating setups, like an open-ended wind tunnel, it can be a severe issue in recirculating (closed) setups, e.g. a TC apparatus, a rotating drum, or a Rayleigh–Bénard cell [18]. For a large range of Reynolds numbers it is known that vortices will be shed [19] from these probes, either

in the form of a Kármán vortex street or as a turbulent wake, depending on the geometry and Reynolds number. These vortices can survive a full revolution, which has been observed in rotating drum experiments [20].

The TC setup used in the present work, the Twente Turbulent Taylor–Couette (T³C) [21–23], distincts itself from other setups by many features: variable gap and radius ratio, precise temperature control, independently rotatable cylinders, and a fully optically accessible gap. The outer cylinder is constructed from 2.5 cm thick PMMA (*Poly-(methyl methacrylate)*), which enables optical measurement techniques, e.g. Particle Tracking Velocimetry (PTV) [24,25], Particle Imaging Velocimetry (PIV) [26,27], and Laser Doppler Anemometry (LDA) [28,29]. These methods, by their very nature, will not disturb the flow under consideration. In addition these techniques are able to measure the velocity components and are directionally sensitive, such that they are capable of detecting flow reversals. The addition of seed particles is imperative for these techniques, and one should check if these particles accurately reflect the velocity of the flow, as discussed below. Additionally, particles should not change the dynamics of the flow, in particular, some particles act as a surfactant in two-phase flows [30–32].

2. Laser Doppler anemometry

LDA is based on the Doppler effect. The most common version of LDA, is a so-called dual beam heterodyne configuration [29], see Figs. 2 and 3. In this configuration two beams are crossed and focused in the flow, creating an interference pattern. Seed particles, added to the flow, passing through the interference pattern will

* Corresponding authors.

E-mail addresses: s.g.huisman@utwente.nl (S.G. Huisman), c.sun@utwente.nl (C. Sun).

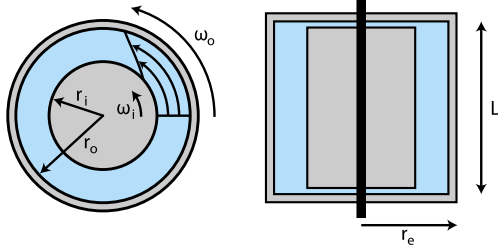


Fig. 1. *Left:* Top view of TC apparatus, two concentric cylinders are rotating. Control parameters are the rotation rates ω_i and ω_o , where the subscripts denote inner cylinder and outer cylinder, respectively. The inner cylinder has a radius of $r_i = 20$ cm, and the outer cylinder has an inner-radius of $r_o = 28$ cm. *Right:* Vertical cross section of a TC apparatus. The outer cylinder has an outer-radius of $r_e = 30.5$ cm and a height $L = 92.7$ cm. The outer cylinder is made from optically transparent PMMA (Poly-(methyl methacrylate)), and is attached to the top and bottom end plates.

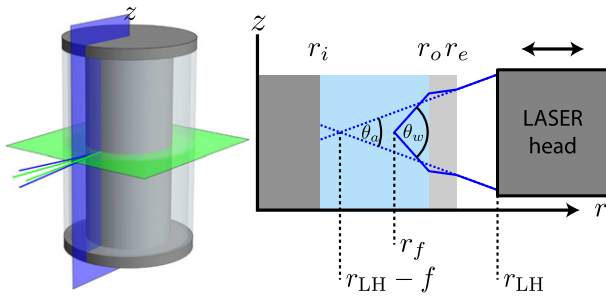


Fig. 2. *Left:* The azimuthal and axial components of the velocity are measured, laser beams are in the green and blue planes respectively. *Right:* Vertical cross section showing two laser beams. The dashed lines are beams *without* refraction, the angle between the beams is denoted θ_a , where *a* stands for air. The solid lines are beams *with* refraction, θ_w is the angle between the beams in water. r_{LH} is the position of the laser head and $r_{LH} - f$ is position of the focus without refraction, while r_f is the real position of the focus. (For interpretation of the references to colour in this figure legend, the reader is referred to the web version of this article.)

scatter light with a specific frequency. This light is then captured by a photo detector and converted to a current from which the Doppler shift can be calculated. Knowing the optical geometry of the setup one can directly calculate the velocity from the Doppler shift [29]:

$$f_d = \frac{2 \sin(\theta/2)}{\lambda} |v_k| \quad (1)$$

where f_d is the Doppler shift, λ the wavelength of the laser, θ the angle between the beams, and v_k the component of the velocity along $\mathbf{k}_1 - \mathbf{k}_2$, where \mathbf{k}_i are the propagation vectors of the laser beams. To add directional sensitivity one has to frequency shift one of the beams, accomplished by a Bragg cell. More details about the Bragg cell, the fringe-model, and LDA in general, can be found in e.g. Refs. [29,33].

Laser Doppler anemometry is a so-called absolute measurement method and therefore does not require calibration against a known flow. This, however, does not mean that a measurement of velocity is error free. Any misalignment in the optical arrangement, and any imperfection in the lenses (e.g. astigmatism [34]) will cause errors. In addition, any particle traveling through the beams prior to focussing can have adverse effects on the formation of a well-defined measurement volume. Similarly, any spatial inhomogeneity of the refractive index causes the focal point to shift, and the waists to mismatch in the measurement volume [35]. Furthermore, the number of particles in the interference zone fluctuates; particles move in and out the measurement volume and induce noise in the collected signal.

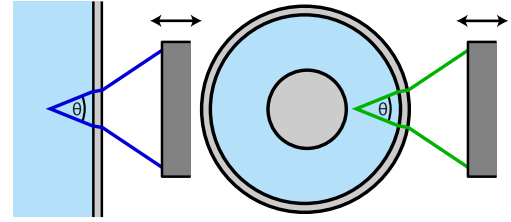


Fig. 3. *Left:* Typical geometry of LDA, equivalent to the vertical plane in the current application. The beams are passing through flat interfaces, and θ does not vary with laser-head position. *Right:* Horizontal plane: laser beams are affected by the curved interfaces, and therefore θ is a function of radial position.

2.1. Curvature effects

In most LDA applications the laser beams travel through flat surfaces, see Fig. 3. In this case, Eq. (1) can be simplified by invoking Snell's law:

$$\frac{f_d}{2|v_k|} = \frac{\sin(\theta_w/2)}{\lambda_w} = \frac{\sin(\theta_a/2)}{\lambda_a} \quad (2)$$

where quantities with *a* subscripts denote quantities in air, and *w* in water. Eq. (2) is only applicable if the interfaces are flat and the optical axis is perpendicular to those interfaces; it is only then that $\theta_a/2$ is the angle of incidence and $\theta_w/2$ the angle of refraction. The difference in refractive index is absorbed by the changing wavelength. So for the case of flat interfaces, θ_a can be obtained from the focal length and the beam separation, and together with λ_a , given by the laser, the velocity can be calculated from the Doppler shift (Eq. (2)). Note that the refractive indices of the container and water are irrelevant; they are not used in the calculation of the velocity.

For the case of a curved surface, see Fig. 3, Eq. (2) does not hold. For this case Snell's law cannot (easily) be applied in order to transform θ_w to θ_a . A prerequisite of calculating the correct velocity is therefore the knowledge of θ_w as a function of gap-position.

Most commonly the calculation of the velocity is implemented in the supplied software and implicitly assumes Eq. (2) to hold. For the case of curved interfaces this equation does not hold, and therefore the measured velocity has to be corrected by multiplying it with a correction factor C_θ :

$$C_\theta = \frac{u_{\phi, \text{real}}}{u_{\phi, \text{measured}}} = \frac{n_a \sin(\theta_a/2)}{n_w \sin(\theta_w/2)}, \quad (3)$$

where *a* subscripts denote quantities in air, and *w* in water; see also Fig. 2.

3. Solutions

The problem at hand is predominantly solved by mounting prisms (see e.g. [36]) to the outer cylinder of the TC apparatus, or by putting the entire apparatus inside a liquid bath (see e.g. [37]) with flat windows. The latter has two purposes: the liquid bath can act as a coolant and match the refractive index of the working fluid. In this way the beams travel through the outer cylinder with less deflection; this solution is, however, not perfect because of the finite thickness of the outer cylinder. Matching the refractive indices of the working fluid, the liquid bath, and the outer cylinder does solve the issue, but becomes cumbersome for large scale devices, or impossible if the studied fluid is a gas. The use of prisms is tantamount to the use of a liquid bath, and is also unable to fully correct for the problem. Furthermore, applying prisms is technically demanding once the outside is in motion. Theoretically one can derive the trajectories of the laser light. Ref. [38] derives these trajectories and even finds simplifications

Table 1

Parameters describing the optical geometry of the presently used Taylor–Couette apparatus: the T³C [21].

Parameter	Symbol	Value (m)
Radius inner cylinder	r_i	0.20
Inner-radius outer cylinder	r_o	0.28
Outer-radius outer cylinder	r_e	0.305
Refractive index PMMA	n_{PMMA}	1.49
Refractive index water	n_{water}	1.333

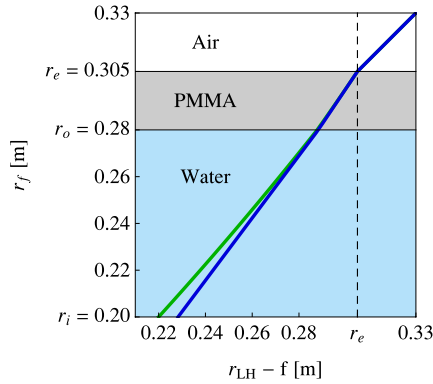


Fig. 4. The position of the two foci as a function of the position of the laser-head. Colors are in accordance with Fig. 2. The trajectory of the blue focus (bottom line) can be described by a piece-wise linear function, while for the green focus it deviates from a linear function due to the curvature of the interfaces. The foci diverge once $r_{\text{LH}} - f < r_e$. (For interpretation of the references to colour in this figure legend, the reader is referred to the web version of this article.)

for the solutions found. This analysis is, however, not complete, as it only considers 1 plane of refraction; the inside of the outer cylinder. In our application our cylinder is very thick compared to our measurement range; the gap of our apparatus is 8 cm versus a cylinder of thickness 2.5 cm. Here we will consider both interfaces, and calculate the trajectories by using a ray-tracer, and we will show that taking into account both interfaces is *crucial* for our experiments. Utilizing a ray-tracer has several advantages compared to a theoretical derivation for the present experimental setup (e.g. Ref. [38]): a theoretical derivation becomes cumbersome if one tries to find a formula after more than one refraction. The T³C system will be equipped with multiple outer cylinders to alter the gap-width, a ray-tracer is then more generalized and is able to handle multiple interfaces. The next section describes the use of a ray-tracer in order to account for the effects of the curved interfaces.

4. Ray-tracer

A 3D ray-tracer is built in order to calculate two parameters: the angle θ_w for the green beam pair in the horizontal plane, and the position of the crossings of the blue and green beam pairs in the vertical and horizontal plane, respectively. For the blue beam pair (in the axial–radial plane), the curvature effects does not affect the flow velocity measurements, and therefore Eq. (2) is applicable; the axial velocity does not require correction. The azimuthal velocity, however, does need correction.

The ray-tracer is based on simple principles: starting at point \mathbf{p}_i with direction \mathbf{k}_i , it checks which interfaces are hit for some $t > 0$ at position $\mathbf{p}_i + t\mathbf{k}_i$. The next point in the ray-trace can be defined from the interface that is hit first: $\mathbf{p}_{i+1} = \mathbf{p}_i + t_{\min}\mathbf{k}_i$. The normal of this interface is calculated at position \mathbf{p}_{i+1} , and is denoted $\hat{\mathbf{s}}$, where the hat means the vector has unit length. For the case of reflection the new direction is given by

$$\hat{\mathbf{k}}_{i+1} = \hat{\mathbf{k}}_i - 2(\hat{\mathbf{k}}_i \cdot \hat{\mathbf{s}})\hat{\mathbf{s}}. \quad (4)$$

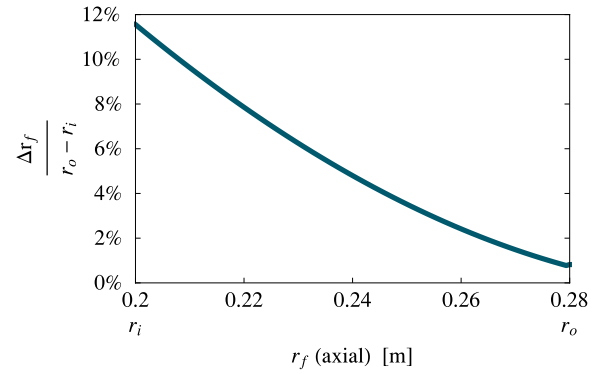


Fig. 5. The separation between the measurement positions is normalized with the gap width and plotted versus the focal position of the ‘axial’ beams. Near the inner cylinder the distance between the two foci is the highest and constitutes more than 11% of the gap. Due to the thickness of the outer cylinder there is non-zero distance between the two foci when focused at $r = r_o$.

For the case of refraction, Snell's law:

$$n_i(\hat{\mathbf{k}}_i \times \hat{\mathbf{s}}) = n_{i+1}(\hat{\mathbf{k}}_{i+1} \times \hat{\mathbf{s}}), \quad (5)$$

is solved for \mathbf{k}_{i+1} under the constraint that it has unit length and in the plane spanned by $\hat{\mathbf{s}}$ and $\hat{\mathbf{k}}_i$. This can be implemented without the use of trigonometric functions, which can be troublesome in certain fringe cases; see the Appendix for more details.

Once the new position and new direction are found, the algorithm can be repeated until it exits the apparatus, or until it is absorbed by a surface.

This algorithm has been applied to the geometry of our LDA and TC setup. Our focal length $f = 0.5$ m, our beam separation is 76 mm for the green beams, and 73 mm for the blue beams. The optical geometry of the TC apparatus used in the present work [21] can be characterized by 3 radii and 3 refractive indices; see Figs. 1 and 2 and Table 1.

4.1. Shift of focal position

In this section the location of the foci (*i.e.* the measurement position) for both pairs of beams are calculated. The position of the laser-head r_{LH} is varied, see Fig. 2. The focal position of the undisturbed beams is given by $r_{\text{LH}} - f$. For each beam-pair the focal position r_f is calculated as a function of r_{LH} , see Figs. 2 and 4.

If the focus is outside the apparatus, *i.e.* $r_{\text{LH}} - f > r_e$, the focal position is given by $r_f = r_{\text{LH}} - f$. If the laser head is moved inward (decreasing $r_{\text{LH}} - f$) the beams will first hit the outer cylinder at $r_f = r_e = r_{\text{LH}} - f$. Moving the laser head further inward will cause the foci to lie inside the PMMA, and moving even further, inside the water. The blue beams are in the azimuthal–radial plane and refract differently from beams traveling in the axial–radial plane. The focus of the blue beams hits the inner cylinder ($r_f = r_i$) at $r_{\text{LH}} - f \approx 0.228$ m, while the focus of the green beams hits the inner cylinder at $r_{\text{LH}} - f \approx 0.22$ m. The distance between the two foci as a function of the radial position is depicted in Fig. 5.

A pronounced shift of the focal positions is observed, see Fig. 5; the foci never coincide, and the maximum separation is 11.5% of the gap. The effects due to curved interfaces can therefore not be neglected. Furthermore, note that the foci do not even coincide at $r = r_o$; this is due to the finite thickness of the outer cylinder, it is therefore necessary to consider both interfaces in the analysis.

4.2. Beam angle correction

For the case of flat surfaces (the axial–radial plane) the velocity calculated by the supplier's software does not have to be corrected. Eq. (2), however, does not hold in the azimuthal–radial plane due to the curved surfaces, and the velocity has to be corrected

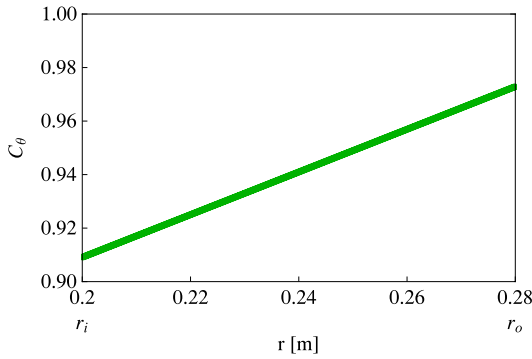


Fig. 6. Correction factor C_θ (see Eq. (3)) as a function of the radial position r . The azimuthal velocity u_ϕ has to be corrected: $u_{\phi,\text{real}} = C_\theta(r)u_{\phi,\text{measured}}$.

by multiplication with C_θ , see Eq. (3). The refractive indices are known, and θ_a can be found from the focal length and the beam separation. θ_w can be found by calculating the angle between the focussing rays, see Figs. 2 and 3. The correction factor can then be calculated, see Fig. 6.

The velocity has to be corrected by 3% to 9%, depending on the radial position. Note that there is a finite correction (about 3% for the optical geometry of the current apparatus) at the water–PMMA interface at $r = r_o$, this is due to the non-zero thickness of the outer cylinder and taking into account both interfaces of the outer cylinder in the analysis.

5. Experimental verification

The results obtained from the ray-tracer can be verified by measuring a known flow state. The temperature of the TC system is kept at 20 °C with water as the working fluid. Dantec polyamide seed particles ($r_{\text{seed}} = 2.5 \mu\text{m}$) with a density of $1.03 \cdot 10^3 \text{ kg/m}^3$ are used. One can estimate the minimum velocity difference $\Delta v = |v_{\text{seed}} - v_{\text{fluid}}|$ between a particle v_{seed} and its surrounding fluid v_{fluid} needed for the drag force $F_{\text{drag}} = 6\pi\mu r_{\text{seed}}\Delta v$ to outweigh the centrifugal force $F_{\text{cent}}(r) = \frac{4}{3}\pi r_{\text{seed}}^3(\rho_{\text{seed}} - \rho_{\text{fluid}})\frac{v_r^2}{r}$. A typical velocity in the middle of the gap ($r = 0.24 \text{ m}$) is $v = 5 \text{ m/s}$, combining with the density and viscosity of water around 20 °C, resulting in $\Delta v \approx 4 \times 10^{-6} \text{ m/s}$. This is several orders of magnitude smaller than the typical velocity fluctuation inside the TC-gap of order 10^{-1} m/s and hence centrifugal forces on the seeding particles are negligible.

For TC flow a stable and well-known flow state is solid body rotation; the inner and outer cylinder are both rotated at a fixed speed ω . After sufficient waiting the fluid will have a velocity $u_\phi = \omega r$, and $u_z = u_r = 0$. The experiment has been performed for three rotation rates ω ($\omega/2\pi = 1 \text{ Hz}$, 2 Hz , and 4 Hz), where the azimuthal velocity has been measured at several radial positions and at mid height. Similar results were found for all three cases, Fig. 7 shows the results for the case of $\omega/(2\pi) = 2 \text{ Hz}$.

The measured velocities are shown in red squares, after applying the beam angle correction the data points (blue circles) are found to agree with the theoretical flow profile within 0.75%. Any remaining deviation can be due to e.g. optical misalignment or imperfection, spatially inhomogeneous refractive index in the working fluid, or noise created by the amplification and digitalization of the optical signal.

6. Application

Here the results are shown for the measurement of the azimuthal velocity profile for the case that the inner cylinder is stationary and the outer cylinder is rotating. This case has been

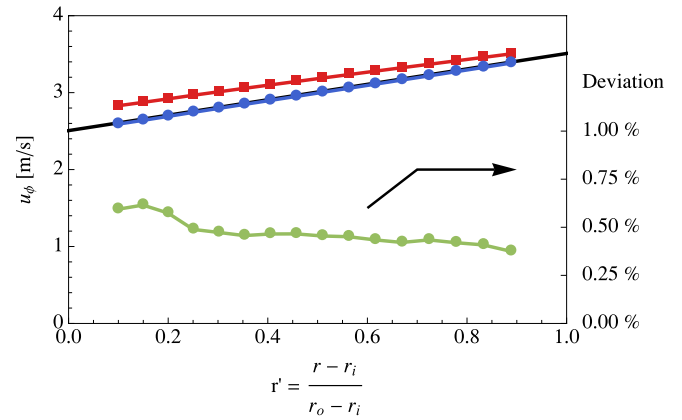


Fig. 7. In red squares the *uncorrected* azimuthal velocity as a function of radial position is shown, and in blue dots the *corrected* azimuthal velocity. The black solid line is the theoretical flow profile $u_\phi = \omega r$, the deviation from this profile is plotted with green dots, the corresponding scale is on the right. The theoretical and corrected measured profiles are found to be in good accordance. (For interpretation of the references to colour in this figure legend, the reader is referred to the web version of this article.)

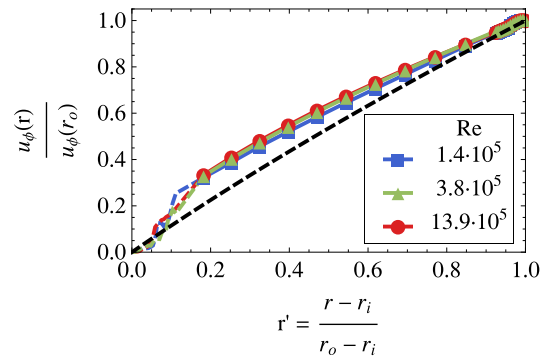


Fig. 8. For three rotation rates the azimuthal velocity is measured along the gap. This velocity is normalized by the driving velocity in order to collapse the data, and compared to the laminar velocity profile for infinite aspect ratio (dashed line). The profile is found to be nearly independent of the Reynolds number.

studied before [12,16], and because the flow is laminar, even for high Reynolds number, any perturbation due to a measuring probe is likely to survive a full revolution. To accurately obtain the speed of the (undisturbed) flow, it has to be measured non-intrusively. Fig. 8 shows the results of three experiments having varying Reynolds number ($\text{Re} = \omega_o r_o (r_o - r_i) / \nu$).

For three rotation rates the obtained profiles are found to collapse over a decade of Reynolds number, but deviate from the laminar velocity profile for infinite aspect-ratio. Due to a finite aspect ratio of the setup the presence of the end plates will create a secondary flow, modifying the azimuthal velocity profile. The velocity close to the inner cylinder is currently unattainable by LDA due to reflections coming of the inner cylinder surface. These reflections create spurious, unreliable data and therefore the profiles are shown dashed in that region. The present system will, in the future, be equipped with a transparent inner cylinder, which will significantly reduce the reflections.

7. Conclusion

In order to measure correct velocities inside a TC apparatus using LDA, one has to correct for the effects of the curved interfaces. Not only do the positions of the measurement volumes depend non-trivially on the position of the laser head, but also the measured velocity has to be corrected. A ray tracer has been used in order to calculate the position of the foci, but also to calculate the

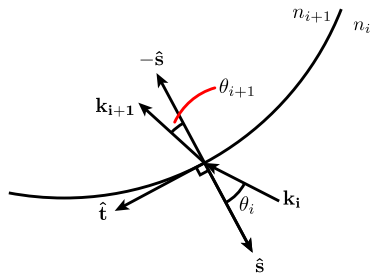


Fig. 9. Sketch of the rays in the plane of refraction.

correction factor C_θ as a function of radial position. We showed that for our application it is crucial to take into account both interfaces of the outer cylinder. The measurement positions do not coincide and the velocity has to be corrected even at $r = r_o$. Our ray-tracer is verified by measuring the velocity for the case of solid body rotation; good agreement with the theoretical prediction has been found. For pure outer cylinder rotation it is found that the velocity deviates from the laminar velocity profile for infinite aspect ratio due to the presence of the end plates.

Acknowledgments

This work was financially supported by technology foundation STW in The Netherlands. Stimulating discussions with Jan Abshagen, René Delfos, Detlef Lohse, Gerd Pfister, Florent Ravelet, and Jerry Westerweel are acknowledged. We also acknowledge the help of G.W. Bruggert, M. Bos and B. Benschop for their technical support.

Appendix

For each interface one has to solve Snell's law $n_i(\hat{\mathbf{k}}_i \times \hat{\mathbf{s}}) = n_{i+1}(\hat{\mathbf{k}}_{i+1} \times \hat{\mathbf{s}})$ for \mathbf{k}_{i+1} . From the vector equation one can see that the solution is not unique; but the solution is unique if we require the solution to be in the plane spanned by $\hat{\mathbf{s}}$ and $\hat{\mathbf{k}}_i$ (called the plane of refraction). In this plane the solution can be rewritten as follows: $n_i \sin(\theta_i) = n_{i+1} \sin(\theta_{i+1})$. \mathbf{k}_{i+1} can be decomposed in two parts; one in the direction of $\hat{\mathbf{s}}$ and one that is tangential to the interface and in the plane of refraction, denoted $\hat{\mathbf{t}}$, see Fig. 9. By simple geometry one can find that $\mathbf{k}_{i+1} = \sin(\theta_{i+1})\hat{\mathbf{t}} + \cos(\theta_{i+1})(-\hat{\mathbf{s}})$. The direction of \mathbf{t} can be found by subtracting the normal component of the incident ray: $\mathbf{t} = \hat{\mathbf{k}}_i - (\hat{\mathbf{k}}_i \cdot \hat{\mathbf{s}})\hat{\mathbf{s}}$. From the definition of the cross product $(\mathbf{a} \times \mathbf{b}) = |\mathbf{a}||\mathbf{b}| \sin(\alpha)$, where α is the angle between vectors \mathbf{a} and \mathbf{b} and Snell's law, one can derive that $\sin(\theta_{i+1}) = \frac{n_1}{n_2} \left| \hat{\mathbf{k}}_i \times \hat{\mathbf{s}} \right|$, and using the Pythagorean identity one writes $\cos(\theta_{i+1}) = \sqrt{1 - \sin(\theta_{i+1})^2}$. Note that one does not need to calculate the angles θ_i or θ_{i+1} , it is only necessary to know the sine and or cosine of the angles. The direction for the outgoing ray can now be found by substituting all the values: $\mathbf{k}_{i+1} = \sin(\theta_{i+1})\hat{\mathbf{t}} + \cos(\theta_{i+1})(-\hat{\mathbf{s}})$.

References

- [1] L. Rayleigh, On the dynamics of revolving fluids, Proc. R. Soc. Lond. Ser. A 93 (1917) 148–154.
- [2] G.I. Taylor, Stability of a viscous liquid contained between two rotating cylinders, Philos. Trans. R. Soc. Lond. A Math. Phys. Eng. Sci. 223 (1923) 289.
- [3] G. Pfister, I. Rehberg, Space dependent order parameter in circular Couette flow transitions, Phys. Lett. 83 (1981) 19–22.

- [4] R.C. DiPrima, H.L. Swinney, Instabilities and transition in flow between concentric rotating cylinders, in: H.L. Swinney, J.P. Gollub (Eds.), Hydrodynamic Instabilities and the Transition to Turbulence, Springer, 1981.
- [5] C.D. Andereck, S.S. Liu, H.L. Swinney, Flow regimes in a circular Couette system with independently rotating cylinders, J. Fluid Mech. 164 (1986) 155.
- [6] M.A. Dominguez-Lerma, D.S. Cannell, G. Ahlers, Eckhaus boundary and wave-number selection in rotating Couette–Taylor flow, Phys. Rev. A 34 (1986) 4956–4970.
- [7] T. Mullin, K.A. Cliffe, G. Pfister, Unusual time-dependent phenomena in Taylor–Couette flow at moderately low Reynolds-numbers, Phys. Rev. Lett. 58 (1987) 2212–2215.
- [8] G. Pfister, H. Schmidt, K.A. Cliffe, T. Mullin, Bifurcation phenomena in Taylor–Couette flow in a very short annulus, J. Fluid Mech. 191 (1988) 1–18.
- [9] D.P. Lathrop, J. Fineberg, H.L. Swinney, Transition to shear-driven turbulence in Couette–Taylor flow, Phys. Rev. A 46 (1992) 6390–6405.
- [10] P. Buchel, M. Lucke, D. Roth, R. Schmitz, Pattern selection in the absolutely unstable regime as a nonlinear eigenvalue problem: Taylor vortices in axial flow, Phys. Rev. E 53 (1996) 4764–4777.
- [11] A. Esser, S. Grossmann, Analytic expression for Taylor–Couette stability boundary, Phys. Fluids 8 (1996) 1814–1819.
- [12] D. Coles, C. Van Atta, Measured distortion of a laminar circular Couette flow by end effects, J. Fluid Mech. 25 (1966) 513.
- [13] G.P. Smith, A.A. Townsend, Turbulent Couette flow between concentric cylinders at large Taylor numbers, J. Fluid Mech. 123 (1982) 187–217.
- [14] G.S. Lewis, Velocity fluctuations, wall shear stress and the transition in torque scaling at $Re = 13\,000$ in turbulent Couette–Taylor flow, Ph.D. Thesis, University of Texas at Austin, 1996.
- [15] G.S. Lewis, H.L. Swinney, Velocity structure functions, scaling, and transitions in high-Reynolds-number Couette–Taylor flow, Phys. Rev. E 59 (1999) 5457–5467.
- [16] F. Wendt, Turbulente Strömungen zwischen zwei rotierenden konaxialen Zylindern, Arch. Appl. Mech. 4 (1933) 577–595.
- [17] J.M. Wallace, P.V. Vukoslavčević, Measurement of the velocity gradient tensor in turbulent flows, Annu. Rev. Fluid Mech. 42 (2010) 157–181.
- [18] G. Ahlers, S. Grossmann, D. Lohse, Heat transfer and large scale dynamics in turbulent Rayleigh–Bénard convection, Rev. Math. Phys. 81 (2009) 503.
- [19] R. King, A review of vortex shedding research and its application, Ocean Eng. 4 (1977) 141–171.
- [20] C. Sun, T. Mullin, L. van Wijngaarden, D. Lohse, Drag and lift forces on a counter-rotating cylinder in rotating shear flow, J. Fluid Mech. 664 (2010) 150–173.
- [21] D.P.M. van Gils, G. Bruggert, D.P. Lathrop, C. Sun, D. Lohse, Twente turbulent Taylor–Couette (T^2C): strongly turbulent two-phase flow between independently rotating cylinders, Rev. Sci. Instrum. (2011).
- [22] D.P.M. van Gils, S.G. Huisman, G. Bruggert, C. Sun, D. Lohse, Torque scaling in turbulent Taylor–Couette flow with co- and counterrotating cylinders, Phys. Rev. Lett. 106 (2011).
- [23] S.G. Huisman, D.P.M. van Gils, S. Grossmann, C. Sun, D. Lohse, Ultimate turbulent Taylor–Couette flow, Phys. Rev. Lett. 108 (2012) 024501.
- [24] H.G. Maas, A. Gruen, D. Papantoniou, Particle tracking velocimetry in three-dimensional flows, Exp. Fluids 15 (1993) 133–146.
- [25] N. Ouellette, H. Xu, E. Bodenschatz, A quantitative study of three-dimensional Lagrangian particle tracking algorithms, Exp. Fluids 40 (2006) 301–313.
- [26] M. Raffel, C. Willert, S. Wereley, J. Kompenhans, Particle Image Velocimetry: A Practical Guide, Springer, 2007.
- [27] F. Ravelet, R. Delfos, J. Westerweel, Influence of global rotation and Reynolds number on the large-scale features of a turbulent Taylor–Couette flow, Phys. Fluids 22 (2010) 055103.
- [28] Y. Yeh, H.Z. Cummins, Localized fluid flow measurements with an He–Ne laser spectrometer, Appl. Phys. Lett. 4 (1964) 176–178.
- [29] H.-E. Albrecht, M. Borys, N. Damaschke, C. Tropea, Laser Doppler and Phase Doppler Measurements Techniques, Springer, 2003.
- [30] R.E. Davis, A. Acrivos, The influence of surfactants on the creeping motion of bubbles, Chem. Eng. Sci. 21 (1966) 681–685.
- [31] R.M. Griffith, The effect of surfactants on the terminal velocity of drops and bubbles, Chem. Eng. Sci. 17 (1962) 1057–1070.
- [32] R.B. Fdhila, P.C. Duineveld, The effect of surfactant on the rise of a spherical bubble at high Reynolds and Peclet numbers, Phys. Fluids 8 (1996) 310–321.
- [33] L. Drain, The Laser Doppler Technique, J. Wiley, 1980.
- [34] Z. Zhang, K. Eisele, The effect of astigmatism due to beam refractions on the formation of the measurement volume in LDA measurements, Exp. Fluids 20 (1996) 466–471.
- [35] C. Resagk, R. Puits, A. Thess, Error estimation of laser-doppler anemometry measurements in fluids with spatial inhomogeneities of the refractive index, Exp. Fluids 35 (2003) 357–363.
- [36] L.D. Castello, Table-top rotating turbulence: an experimental insight through particle tracking, Ph.D. Thesis, Eindhoven University of Technology, The Netherlands, 2010.
- [37] C. Sun, K.-Q. Xia, P. Tong, Three-dimensional flow structures and dynamics of turbulent thermal convection in a cylindrical cell, Phys. Rev. E 72 (2005) 026302.
- [38] Z. Zhang, Optical guidelines and signal quality for LDA applications in circular pipes, Exp. Fluids 37 (2004) 29–39.